Resonant Saturable Absorber Mirrors for Dispersion Control in Ultrafast Lasers

Mathias Moenster, Uwe Griebner, Wolfgang Richter, and Günter Steinmeyer, *Member, IEEE*

***Abstract*—We discuss a concept for incorporating dispersion compensation into a saturable absorber mirror. This integrated device relies on an absorber layer embedded in a resonator structure and can provide negative dispersion of several 1000 fs^2, similar to the spectral phase characteristics of a Gires–Tournois interferometer. A similar integration is possible also for semiconductor gain structures, as they are employed in semiconductor disk lasers. We will provide a detailed analysis of the dispersion compensation capacities of our approach, linking dispersion scaling and nonlinear properties of the device. The theoretical part will be illustrated by dispersion measurements on prototypical devices. We believe that our concept paves the way for fully integrated vertical semiconductor femtosecond lasers but may also find numerous applications in solid state lasers and femtosecond fiber lasers.**

***Index Terms*—Group delay dispersion, passive mode-locking, photonic switching, photonic thin-film devices, saturable absorber mirrors.**

I. Introduction

ULTRAFAST lasers have greatly benefitted from the development of two thin-film devices, the saturable-absorber mirror and dielectric mirrors for dispersion compensation. Saturable absorber mirrors (SAMs) [1]–[6] have become a key element for mode-locking all-solid-state lasers. They rely on the nonlinearity of a semiconductor quantum well, and their response can be tailored in wavelength and saturation fluence for the requirements in a particular laser. Introducing defects into the structure, the relaxation of the quantum well can be suitably accelerated to generate pulses of picosecond duration well down into the femtosecond range. Dispersive dielectric mirrors are nonabsorptive structures that have greatly enhanced the capacities for intra-cavity dispersion compensation in mode-locked lasers. One example for such dispersive mirrors is the chirped mirror [7], [8]. The dispersion of a chirped mirror relies on the wavelength-dependent penetration depth of the light within a mirror stack with graded Bragg wavelength. Chirped mirrors enable wideband dispersion compensation over bandwidths up to about one optical octave, i.e., much more than is possible with prism arrangements. A second type of dispersion compensating mirror is a thin-film variant of the Gires–Tournois interferometer (GTI) [9]. The GTI is an all-pass interferometer that consists of two mirrors, one partial reflector and a highly reflecting mirror at a fixed spacing d. Obviously such an arrangement reflects all light without affecting its amplitude but modifies the spectral phase of the reflected light. This phase change is periodic in frequency with a periodicity similar to the phase of a Fabry–Perot interferometer. Such GTI mirrors have been used for intracavity dispersion compensation earlier than chirped mirrors [10]–[12]. They can deliver large amounts of group delay dispersion for bandwidths up to a few ten nanometers. In the following, we will analyze how to combine saturable absorption and the dispersion properties of a GTI-like device in one monolithic semiconductor structure. This approach has already been demonstrated for the generation of 160-fs pulses from a Cr:LiSAF laser [13]. This device provided a -400 fs^2 dispersion compensation over a $\approx$20-nm bandwidth. Similar devices have been considered for noise suppression and dynamic dispersion compensation in telecom systems [14]. Despite these earlier demonstrations, we believe that the full utility of the resonant saturable absorber mirror (RSAM) for generating large amounts of dispersion and its usefulness, e.g., for fiber lasers [15], [16] and vertically integrated semiconductor lasers [17]–[20] has not yet been realized. Furthermore we will also discuss how to incorporate gain rather than absorber sections into a GTI resonator, which constitutes an important step towards a fully integrated mode-locked semiconductor laser.

II. Phase Response of a Resonant Saturable Absorber Mirror

The structure of the device under consideration is depicted in Fig. 1. This device may either be considered as a GTI with added absorber section or as the limiting case of an asymmetric Fabry–Perot interferometer with the reflectivity of one mirror approaching unity. The structure consists of a partial reflector M1, displaying an amplitude reflectivity r, and a highly reflecting mirror M2, with one or several absorber layers between M1 and M2. For simplicity, we will assume that the space between M1 and M2 is homogeneously filled by an absorptive material with complex refractive index $n + i\kappa$. The extinction coefficient κ relates to the linear power absorption coefficient α as $\alpha = 4\pi\kappa/\lambda$, where λ is the vacuum wavelength. Given a mechanical spacing d between mirrors M1 and M2, the round-trip amplitude transmission t through the absorber structure amounts to

$$t = \exp(-\alpha d) \approx 1 - \frac{4\pi\kappa d}{\lambda}. \tag{1}$$

Power losses amount to $A = 1 - t^2$ per round-trip in the resonant cavity. Other than a conventional GTI, the device in Fig. 1 displays wavelength dependent losses, even when we assume

Manuscript received September 5, 2006. This work was supported in part by the German Federal Ministry of Economics and Technology under Project IW051031.

M. Moenster, U. Griebner, and G. Steinmeyer are with the Max-Born-Institut für Nichtlineare Optik und Kurzzeitspektroskopie, D-12489 Berlin, Germany (e-mail: steinmey@mbi-berlin.de).

W. Richter is with BATOP GmbH, D-99425 Weimar, Germany (e-mail: info@batop.de).

Digital Object Identifier 10.1109/JQE.2006.889056

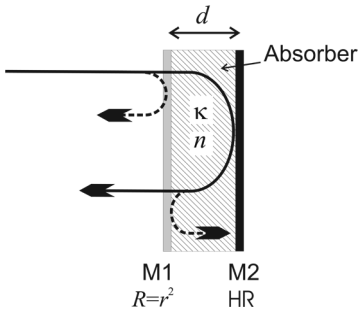

Fig. 1. Structure of a resonant saturable absorber mirror (RSAM). The mirror consists of an absorber section with refractive index $n+i\kappa$, embedded between a partial reflector M1 with power reflectivity R and a high reflector (HR) M2 with 100% reflectivity. A pulse entering this structure experiences two major reflections, creating a leading and a sequence of trailing satellite pulses, as schematically indicated by the dashed arrows.

no spectral dependence of κ and n. The device response is calculated similar to the case of the GTI, however, augmenting the unity-amplitude phase factor $\exp[i\psi(\omega)]$ by the additional factor t previously introduced. The amplitude reflectivity of the device is then written as

$$r_{dev}(\omega) = \frac{r - t\exp[i\psi(\omega)]}{tr\exp[i\psi(\omega)] - 1} \tag{2}$$

with the interferometer phase

$$\psi(\omega) = -\omega\tau = -\frac{2nd\omega}{c} \tag{3}$$

i.e., the linear response of the device is periodic with respect to ω at a period $c/2nd$, as is a Fabry–Perot interferometer or regular GTI. We can separate the response function (2) into amplitude and phase, yielding the spectrally dependent power reflectivity

$$R(\omega) = \frac{t^2 - 2tr\cos\psi + r^2}{t^2r^2 - 2tr\cos\psi + 1} \tag{4}$$

and the phase response

$$\varphi_{dev}(\omega) = \tan^{-1}\left[\frac{t(r^2-1)\sin\psi}{(t^2+1)r - t(r^2+1)\cos\psi}\right]. \tag{5}$$

In resonance, i.e., at $\psi = 2N\pi$ with $N \in \mathbb{N}$, the device provides minimum reflectivity

$$R_{\min} = \left(\frac{t-r}{tr-1}\right)^2 \tag{6}$$

whereas the reflectivity increases to

$$R_{\max} = \left(\frac{t+r}{tr+1}\right)^2 \tag{7}$$

in antiresonance $[\psi = (2N+1)\pi]$. One can convince oneself that $R_{\min} = R_{\max} \equiv 1$ in the limiting case $t = 1$, i.e., the device exhibits all-pass characteristics for vanishing absorption. One may further notice that a vanishing numerator in (6) will result in total extinction in resonance for the case $t = r$. This case of matched impedance allows for a deep modulation and has been extensively analyzed for electro-absorptive modulators embedded in asymmetric Fabry–Perot cavities, see, e.g., [21], [22]. A similar condition in waveguide-ring resonator systems has also been explored for optical switching applications and was termed critical coupling [23]. In the following, we will refer to the condition $t = r$ as critical absorption. For application as a passive mode-locker, (6) and (7) enable tailoring of the saturation fluence and modulation depth of the device by either increasing or decreasing coupling between the light field and the quantum wells of the absorber.

The dispersion properties of an RSAM structure can be obtained from differentiating (5) with respect to ω

$$\begin{aligned} D_2 &= \frac{d^2\varphi_{dev}}{d\omega^2} \\ &= \tau^2 r(1-r^2)\sin\psi \\ &\quad \times \frac{\gamma\left[r^4+(8+2\cos 2\psi-\gamma^2)r^2+1\right]-8r(r^2+1)\cos\psi}{\left[r^4+(\gamma^2+2\cos 2\psi)r^2+1-2\gamma r(r^2+1)\cos\psi\right]^2} \end{aligned} \tag{8}$$

where we have defined $\gamma = t + t^{-1}$. At first sight, (8) may not look very inspiring. Closer inspection of this equation, however, reveals some interesting properties of the dispersion characteristics of an RSAM. To illustrate this, Fig. 2 shows a sequence of dispersion characteristics for constant t but differing values of r. Far away from the critical condition $t = r$ and for t close to unity, the group delay dispersion is reasonably well approximated by sinusoidal behavior

$$D_2 \approx 2\tau^2 r(r+1)\left[\frac{r-1}{(r-t)(1-tr)}\right]^3 \sin\psi \tag{9}$$

with respect to frequency. The case of lowest $r = 0.1$ in Fig. 2(b) illustrates this scenario of spurious dispersion. For the case of small absorption $(0.9 < t < 1)$, as typically encountered in single quantum well designs, (9) is useful to directly determine the magnitude of dispersion oscillations [24]. Typically, dispersion oscillations can be neglected for antireflection coated SAMs $(r < 0.1)$, but may already amount to substantial amplitude for uncoated semiconductor surfaces $(r = 0.5\text{–}0.7)$, as indicated by the second trace in Fig. 2(b), which corresponds to the reflectivity of an uncoated semiconductor front facet. For the case shown, dispersion oscillations already amount to an amplitude of 50 fs^2, i.e., the equivalent of about 2 mm of silica glass. Moreover, the dispersion characteristics already strongly deviate from a simple sinusoid. This parasitic dispersion contribution must not be confused with Kramers–Kronig contributions from the spectral variation of the quantum well response [17], [25], which will typically be much weaker. With even higher reflectivities, one sees a dramatic increase of dispersion, and the periodic function starts to develop into a third-order pole for $t \to r$ at the resonances $\psi = 2N\pi$, exhibiting a negative spike at wavelengths right below resonance and a second positive one of equal magnitude above the resonance. Simultaneously, the reflectivity of the SAM Fig. 2(a) undergoes a similar transition from a sinusoidal variation of $r(\omega)$ to a function resembling the response of a high-finesse Fabry–Perot interferometer, yet with a much less dramatic increase of modulation depth as compared to the

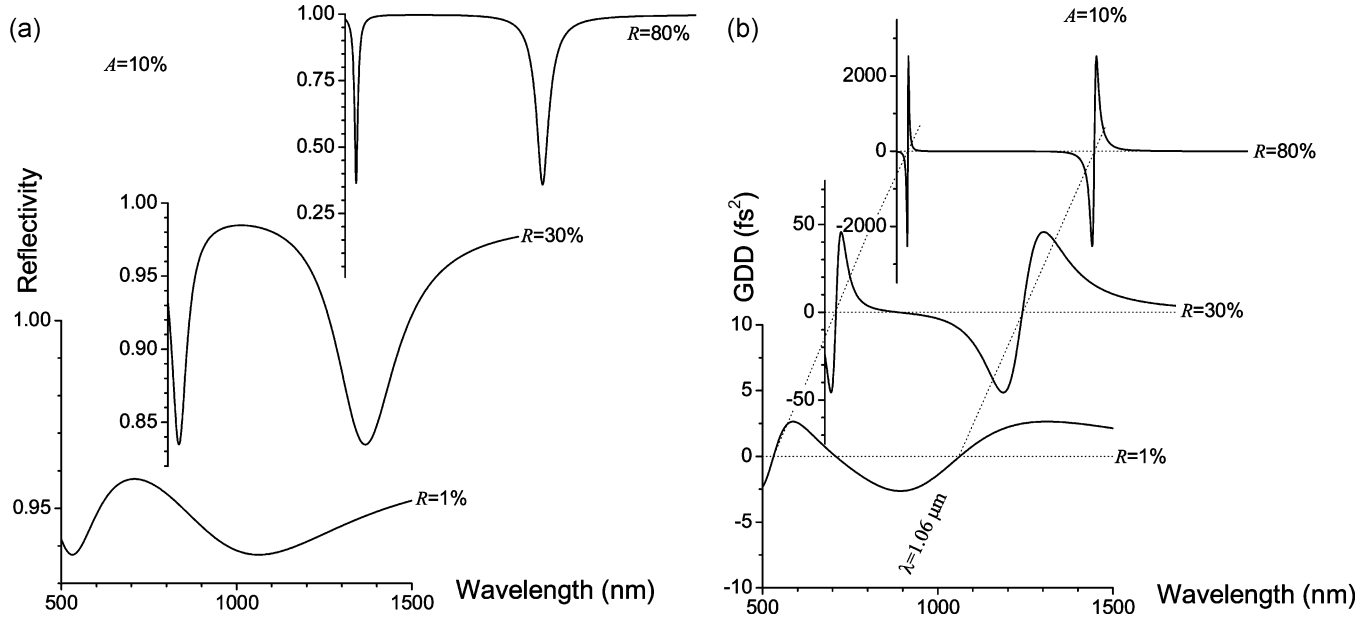

Fig. 2. Reflectivity and dispersion of different SAM devices with differing front reflectivity $r = 0.1, 0.54$, and 0.9, corresponding to the case of an antireflection-coated, an uncoated, and a high-reflectivity coated device, respectively. Other parameters $\tau = 3.5$ fs, and $t = 0.974$ are kept constant. In each subfigure, the bottom trace shows the behavior of an antireflection coated SAM, the middle trace that of an uncoated semiconductor surface, and finally the top trace that of a highly reflecting coating. Vertical axes have been adapted to the amount of reflectivity modulation caused by interference of the front reflection and reflections from the back mirror. Horizonal axes have been shifted with respect to each other, with range and scaling factor kept constant. (a) Reflectivity of the SAMs. (b) Group delay dispersion of the same SAMs as calculated from Eq. (8). The dotted lines indicate zero dispersion and the wavelength of the resonances.

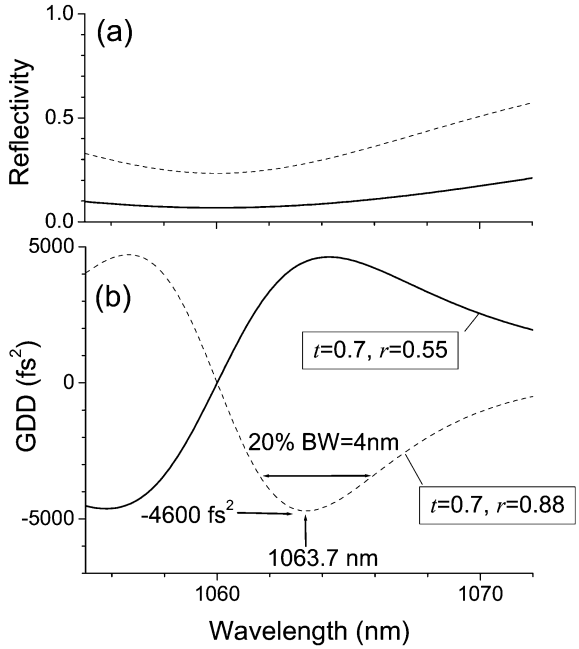

Fig. 3. RSAM designs. Both designs employ $\tau = 21.2$ fs and $t = 0.7$. Dashed line: $r = 0.55 < t$. Solid line: $r = 0.88 > t$. (a) Reflectivity versus wavelength. (b) Dispersion characteristics. Center wavelength, bandwidth, and peak negative dispersion are indicated in the graph.

magnitude of dispersion oscillations in Fig. 2(b). Beyond the critical condition $t = r$, the wavelength dependence of the spiked dispersion characteristics will invert, now exhibiting strong negative dispersion below resonance and positive above. This behavior is illustrated in Fig. 3.

In the immediate vicinity of the resonances, one can reasonably well approximate the GDD of an SAM by a polynomial of odd order. For the case $|t - r| < t/2$, this allows estimates for the position and the value of the maxima, approximating (8) by a third-order polynomial. Using this simplification, the GDD reaches a peak value

$$D_{2,\max} \approx 3.9 \left(\frac{\tau t^3}{r-t}\right)^2 \left[6t^4 + (r-t)(2r-2t-3t^2)\right]^{-2} \tag{10}$$

$$\approx 0.65 \left(\frac{\tau t}{r-t}\right)^2 \tag{11}$$

at detuning

$$\Delta\psi \approx 0.6 \frac{r-t}{t} \tag{12}$$

from resonance. For designing RSAMs it is important to understand that maximum dispersion does not appear on resonance but slightly detuned, whereas third-order dispersion with vanishing second-order contributions is generated directly on resonance. Both estimates, (11) and (12), have already been corrected for a small but systematic underestimation due to the approximation by the third-order polynomial. Note the symmetry of (8). When maximum dispersion $D_{2,\max}$ is reached at detuning $\Delta\psi$ from resonance, minimum dispersion $D_{2,\min} = -D_{2,\max}$ appears at detuning $-\Delta\psi$. Depending on the sign of $(r-t)$, however, positive dispersion will either appear detuned toward higher or lower wavelengths relative to the resonance. This behavior is illustrated in Fig. 3 with two examples showing nearly equally strong dispersive effects of opposite symmetry,

owing to opposite signs of $(r-t)$. Equation (12) can be used for an estimate of the bandwidth of useful dispersion compensation with an RSAM

$$\Delta\omega \approx \frac{0.75}{\tau}\frac{|r-t|}{t} \tag{13}$$

where we have somewhat arbitrarily presupposed that a 20% reduction of the dispersion peak value be tolerable throughout the bandwidth $\Delta\omega$. Putting (11) and (13) into relation one finally yields

$$D_{2,\max} \approx \frac{1.05}{\Delta\omega^2}. \tag{14}$$

This is an interesting result as, to first order, the achievable dispersion does only depend on the bandwidth but not on the order N the GTI is operated in. In the examples of Fig. 3, peak dispersion values of -4600 fs^2 are reached in a 20% bandwidth of 4 nm at 1064-nm center wavelength. With the parameters indicated, (11) predicts a peak dispersion of -4400 fs^2; (13) a bandwidth of about 5 nm. In most cases, the simple estimates (11) and (13) will suffice for predicting the dispersion properties of near-critical RSAM designs.

III. Resonant Laser Designs

The theoretical description of the previous section can be expanded for the case of resonant laser structures. In this case the absorber section of Fig. 1 is replaced by a gain section, providing a round-trip amplitude gain $g > 1$, and the complex phase factor of the gain section is $g\,\exp[i\psi]$. Equation (8) shows an inherent symmetry, yielding identical results when replacing t by t^{-1}. We can, therefore, adopt the entire treatment of the previous section, only replacing $t = g$ and find a similar scenario of critical gain for $r \rightarrow g^{-1}$, again with the potential of creating large amounts of dispersion in the vicinity of this critical condition. We find an extremum of the device dispersion

$$D_{2,\max} \approx 0.65\left(\frac{\tau g}{g-r}\right)^2 \tag{15}$$

at detuning

$$\Delta\psi \approx 0.6\frac{r-g}{g} \tag{16}$$

i.e., a device with gain rather than loss behaves totally identical to the RSAM described by (11) and (12). As the dispersion of resonant laser designs can be inverted by changing the sign of $(g-r)$, similar to the behavior of SAMs shown in Fig. 3, one can design matching SAM/laser pairs, with nearly opposite dispersion characteristics that practically cancel each other out. Of course, this is only a formal extension of the absorber case, presupposing that the laser does not already lase on the resonator formed by the GTI. Whether and for what parameter range such dispersion compensation is useful is certainly subject to further investigation. Still, these equations open up a perspective for fully integrated and dispersion compensated mode-locked semiconductor lasers.

IV. Dynamic Behavior

In the discussion so far it has been surmised that all SAM parameters t, r, and τ are static. Of course, as the very purpose of a saturable absorber is an in crease of the reflectivity with fluence, one has to also take the influence of a dynamic increase of t, i.e., saturation of the losses, into account. Looking at the dispersion in (11), however, one finds that

$$\left.\frac{dD_{2,\max}}{dt}\right|_{\psi=\Delta\psi} = 1.3\tau^2\frac{tr}{(r-t)^3} \tag{17}$$

which can either be positive or negative, depending on the sign of $(r-t)$. This means that depending on the design of the SAM, one can find two different types of dynamical behavior. If $t < r$ the design will dynamically drive itself further towards criticality when the fluence is increased, which will also lead to an increase of the peak dispersion $D_{2,\max}$. Such supercritical behavior is contrasted by a dynamic decrease of $D_{2,\max}$ with fluence for $r < t$. The latter subcritical case is certainly more commonly encountered, as t will typically be in the range from 0.9 to 1 for a single quantum well design. For example, all cases discussed in Fig. 2 are subcritical designs. Only the use of a highly reflecting front mirror or a strong absorption, e.g., due to the use of multiple quantum wells, leads to supercritical behavior of the SAM. Supercritical behavior is encountered for the $r = 0.88$ case depicted in Fig. 3.

Apart from the obvious dependence on t, laser-induced temperature changes or Kerr-induced refraction changes inside the SAM structure can also lead to detuning of the parameter τ from cold-cavity conditions. To avoid dynamic detuning of an RSAM, changes of the optical path length nd must not induce a change of ψ larger than the bandwidth of the device given by (13). This leads to the following criterion:

$$|\Delta(nd)| \ll \frac{\lambda}{20}\frac{|r-t|}{t} \tag{18}$$

where $\Delta(nd)$ is the change of optical path length induced by temperature changes or the Kerr effect. If we consider a design such as the near-critical design depicted in Fig. 2, we find that $\Delta n \ll 0.02$, a refractive index change that is induced by a 100 K temperature change or a peak intensity on the order of 200 GW/cm^2 in typical semiconductor materials [GaAs, $n_2(\lambda = 1060\text{ nm}) \approx -10^{-13}$ cm^2/W]. The latter conditions can typically not be met without causing optical damage and would require a peak power of $\approx$1 MW, e. g., when focusing to a diameter of 20 μm is assumed. Designs with ten times smaller $|r-t|$, however, may already suffer significantly from temperature detuning and may also show the onset of Kerr detuning at nondestructive intensities in the absorber structure. These considerations set a practical limit for the achievable dispersion in an RSAM structure. We expect that it is not practical to generate dispersion exceeding 10000 fs^2 by much, even if such devices are grown to precompensate some of the dynamic shift. Furthermore it will also be difficult to reproducibly grow such designs.

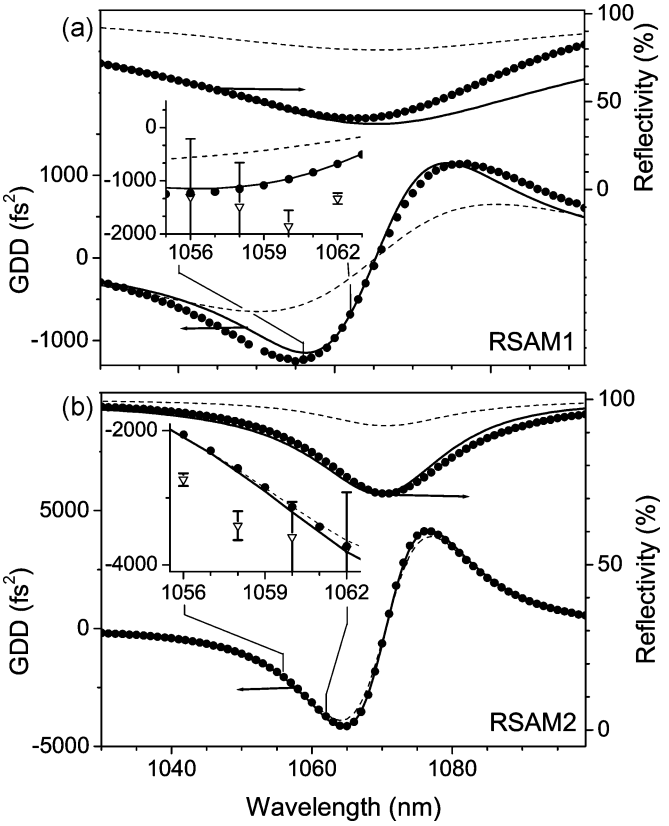

Fig. 4. Reflectivity and dispersion of two RSAMs under test. Solid curves: spectral characteristics as predicted by (4) and (8). (a) RSAM1: $t = 0.78$, $r = 0.5$, $N = 5$. (b) RSAM2: $t = 0.96$, $r = 0.77$, $N = 4$. Dots: spectral characteristics as computed by the matrix method [30], [31]. Dashed curves: calculated dispersion of the fully saturated device, assuming $t = 0.94$ and 0.99 for (a) and (b), respectively. The magnified insets shows a dispersion measurement in comparison with the computed data. Hollow triangles: dispersion measurements by spectral interferometry.

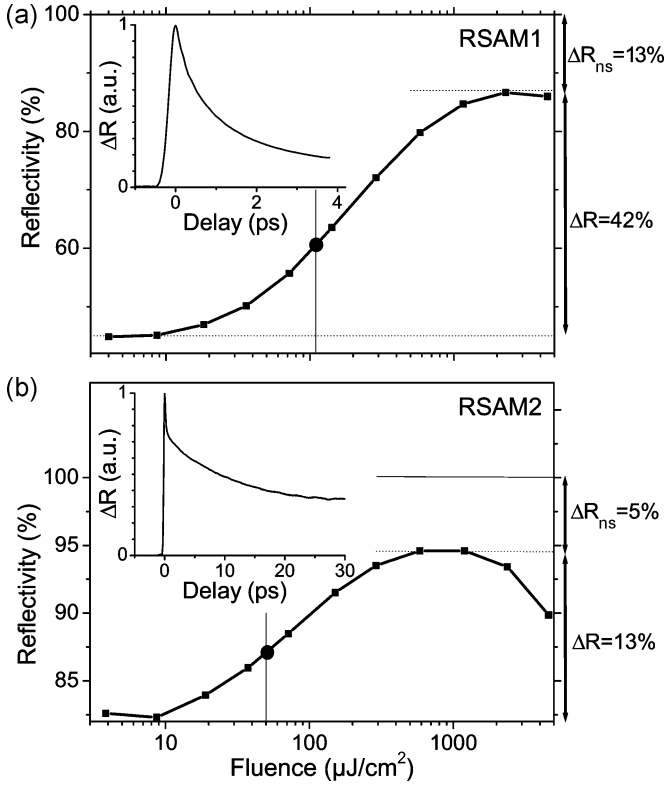

Fig. 5. Reflectivity versus input fluence of the RSAM devices, measured at 1060 nm with a mode-locked Nd:glass laser of 200-fs pulse duration (symbols and solid curve). The saturation fluence $F_{\rm sat}$ was determined with a fitting procedure and is indicated by the filled circle and the thin solid line. Dotted lines indicate how the values for saturable and nonsaturable losses were extracted. The inset shows a pump-probe trace measured with the same laser. (a) RSAM1. (b) RSAM2.

V. Experimental Examples

In the following we will describe an experimental investigation of two manufactured examples for RSAM devices. Both RSAMs are optimized for operation at 1064 nm. In one of these devices two absorber layers are used, with the main goal of providing a substantial saturable loss with a strongly resonant cavity. This cavity is built from 27 layer pair AlAs–GaAs rear mirror, providing a reflectivity of 99.9% and a single protective dielectric half wave layer on GaAs, providing approximately 30% reflectivity. The cavity length corresponds to 2.5λ, i.e., the device is operated in fifth order. In the following, this device will be referred to as RSAM1. The device design data are shown in Fig. 4, both as calculated with a coating design program [30], [31] and as described by the formalism in Section II. Quantum confinement has to be explicitly introduced into transmission matrix calculation. We find that assuming $\kappa = 0.07$ for the extinction coefficient of a quantum well layer gives good agreement with experimental data. As positioning of the absorber layers plays a crucial role for the effective absorption inside the RSAM cavity, this parameter was determined by a fit. The agreement is certainly not perfect, which is mainly caused by spectral variations of the reflectivities and the effective absorption. Still, this comparison confirms that the main characteristics of the device can be described by only three parameters, namely r, t, and the order N.

The saturation fluence of RSAM1 was measured as $F_{\rm sat} = 110\ \mu$J/cm^2, as shown in Fig. 5(a). Despite the rather strong resonant enhancement used in this SAM, this value is comparable to typical values reported for nonresonant devices, see, e.g., [5] and [26]. The modulation depth ΔR of this device amounts to 0.42, which is much larger than the modulation depths of a few percent that are typically reached with nonresonant devices. Non-saturable losses $\Delta R_{\rm ns}$, in contrast, only amount to 0.13. We furthermore conducted pump-probe measurements of this device, which indicate a response time of one to a few ps, as shown in the inset of Fig. 5(a). These measurements indicate that despite the massive use of resonant enhancement, an RSAM does not have to be slow. In fact, the cavity transit times amount to only a few femtoseconds, such that no deterioration is expected down to 100-fs response times.

Design data and characterization measurements of a second RSAM (RSAM2) are shown in Figs. 4(b) and 5(b). This second device has a two layer pair SiO_2–TiO_2 front mirror, providing about 50% reflectivity, and a single quantum well absorber. The device uses the same high reflector as RSAM1 and is operated in fourth order at $\lambda = 1060$ nm. Saturable losses amount to 13%, again with a favorably small value of nonsaturable losses of only 5%. The saturation fluence is 50 μJ/cm^2, i.e., only slightly less than for nonresonant devices. This device shows a bitemporal

behavior, with a fast time constant and a second slower one in the pump-probe response.

While the latter values can be easily extracted by standard measurement techniques [26] it is far more difficult to reliably measure the dispersion properties of the RSAMs. One of the major obstacles is the strong variation of the GDD with wavelength. From the design of the devices, we anticipate a variation of the GDD by a factor two over a wavelength interval of about 5 nm, which makes a high spectral resolution $\delta\lambda < 5$ nm necessary. As it is well known that the standard deviation of a dispersion measurement scales with the third power of the resolution $\delta\lambda$ [27], such a high resolution requires long measurement cycles that are difficult to achieve with traditional white-light interferometry. We substantially reduced data acquisition times by replacing the incandescent light source in our interferometer by a mode-locked Nd:glass laser that exhibits a 10-nm-wide spectrum, with a center wavelength that can be tuned over an 8-nm range. For determining the dispersion, we employed spectral interferometry [28], [29] in a Michelson configuration. Tuning the laser in 2-nm steps, we extracted the spectral dependence of the group delay, as shown in Fig. 4. The measurements were repeated several times to allow for statistical determination of confidence intervals, as indicated by the error bars in Fig. 4. For comparison, the complete design data, i.e., reflectivity and GDD as a function of wavelength are also shown. The measured data may not show perfect agreement with the design data. Still, the measurements confirm that it is in fact possible to generate massive amounts of dispersion with RSAMs. Moreover, the measurements reproduce the magnitude of the dispersion predicted for the particular design and show the expected trend of third-order dispersion, even though the dispersion characteristics may have experienced a small shift due to minimal growth errors. Therefore, this experimental investigation further supports the theoretical model.

Combining the information of the saturation fluence measurements and the dispersion data, one can now go one step beyond, and predict the device behavior in saturation. Assuming that the losses have been reduced to yield the nonsaturable reflectivity values depicted in Fig. 5, one can estimate the reduction of dispersion that goes along with saturating the device. For the two examples shown, the loss L is reduced to about one quarter of the small-signal value $1-\Delta R-\Delta R_{\mathrm{ns}}$, i.e., $L = 1-\Delta R$ in saturation, and $\Delta R/\Delta R_{\mathrm{ns}} \approx 3$. The resulting dispersion characteristics for the saturated case are shown as a dashed line in Fig. 4. Quite interestingly, the dispersion of the two designs shows differing sensitivities towards an increase of t. While the dispersion of RSAM1 is reduced to half of the small-signal value, RSAM2 remains nearly unaffected by the change. This is correctly predicted by (19), indicating a four times higher sensitivity of RSAM1 towards changes of t than for design RSAM2. The examples in Fig. 4 highlight the importance of considering dynamic saturation effects and of computing the robustness of the dispersion towards increasing t already in the design of the devices.

The RSAMs discussed in this Section have already been successfully used in a passively mode-locked neodymium doped microstructure fiber laser [15], [16], operating at a center wavelength of 1.056 μm and yielding pulse durations down to 180 fs in clean soliton operation. In this type of laser with its extremely large gain, it appears to be of paramount importance to provide a passive mode-locking mechanism with large modulation depth ΔR to obtain short pulse durations. Therefore, the best results were obtained with RSAM1. In mode-locked fiber lasers, the dispersion balance is clearly dominated by the microstructure fiber, which displayed a group velocity dispersion $\beta_2 \approx -15$ fs^2/mm in our experiments. This results in a round-trip GDD of -17000 fs^2, i.e., about three times larger than the peak dispersion of RSAM1. In some of our laser experiments, however, we observed deviations from the soliton pulse energies calculated from the fiber dispersion via the soliton area theorem. Similar observations on deviations from predicted soliton energies were previously made by others [32]. Even though dispersion measurements in the saturated case are still outstanding, we believe that the strong dispersion of RSAM2 has modified the intracavity dispersion, enabling higher pulse energies than explainable with the fiber dispersion alone. This further underlines the importance of considering dispersive effects of SAM devices, when using these for passive mode-locking of lasers.

VI. Conclusion

The theoretical treatment and the examples discussed before make it clear that large amounts of dispersion can be generated by RSAM devices. One question that may arise in this context is whether such effects may have gone unnoticed in previous experimental work and whether spurious dispersion effects may explain oddities in the dispersion balance of passively mode-locked lasers. Let us, for example, assume that the semiconductor structure of the SAM had been left completely uncoated. Because of the high index of refraction of semiconductor materials this would lead to amplitude reflectivities $r \approx 0.5$ to 0.7. Given the small absorption of a single quantum well, typical absorption parameters t are in the range 0.95 to 0.99, which identifies a slightly resonant scenario. Assuming a GTI round-trip time $\tau = 4$ fs [5], we calculate an amplitude of the dispersion oscillations of 50 to 150 fs^2, i.e., equivalent to a few millimeters of additional glass in the cavity. Even though such effects are still small, they may already influence the dispersion balance of the cavity and are clearly non-negligible for the performance of the laser in the femtosecond region. If the SAM structure is antireflection coated, this will drive the device out of criticality. Assuming $r = 0.1$, one then finds values of only a few femtosecon square, which can safely be ignored even for the shortest pulses generated with the aid of saturable absorber mirrors [33].

In fact, near-critical conditions can only be met with either additionally coating the SAM surface for higher reflectivity or, alternatively, by using multiple quantum well structures with their higher absorption (smaller values of t). This design approach allows for peak dispersions of thousands of squared femtoseconds, with a bandwidth according to (13). As long as only moderate bandwidths of a few nanometers are required, the RSAM approach easily delivers dispersion compensation for highly dispersive gain materials up to centimeter length and can even supply additional negative dispersion for soliton mode-locking [34]. When designs are driven to dispersion values exceeding ≈ 1000 fs^2, the stability of the design should be carefully examined. Both manufacturing errors and dynamic destabilization

effects may cause a behavior that may deviate significantly from the linear behavior predicted by the analysis of Section II. For larger values of dispersion, therefore, measures may be necessary to precompensate the dynamic behavior of the device. We expect that it will be impractical to produce dispersion values larger than 10000 fs^2, even with careful precompensation.

From a fundamental point of view, it appears interesting to experimentally investigate the dynamical behavior of supercritical RSAM designs. As such devices can theoretically provide a dramatic change of dispersion within the pulse duration, this may lead to interesting pulse shaping effects, caused by the simultaneous increase of peak dispersion and collapse of bandwidth. Similarly, using a second pump pulse in an absorber or changing the gain in a resonant laser device, one could also drive such devices into resonance in a controlled way to investigate the dynamics in the vicinity of critical behavior.

With the formalism developed in this paper, it is easy to predict the dispersive properties of a SAM design, provided the design parameters are at least roughly known. This allows ruling out parasitic dispersion effects in mode-locked solid-state lasers, even when it may prove difficult to directly measure the dispersion of the device. Moreover, a resonant design can often be adapted to provide the same or higher modulation depth as a nonresonant one, but may simultaneously generate negative dispersion, reducing or completely removing the need for dispersion compensating mirrors and prism sequences inside the laser. We think that this is a particular interesting aspect for short-cavity lasers with multigigahertz repetition rates as their cavities do not allow for any other than intrinsic dispersion compensation measures. If semiconductor disk lasers are used, dispersion compensation can also be accomplished inside the gain structure. Ultimately, this may lead to fully vertically integrated laser structures that allow for direct mode-locking without the addition of external elements.

REFERENCES

[1] Y. Silberberg, P. W. Smith, D. J. Eilenberger, D. A. B. Miller, A. C. Gossard, and W. Wiegemann, "Passive mode locking of a semiconductor diode laser," *Opt. Lett.*, vol. 9, pp. 507–509, 1984.

[2] M. N. Islam, E. R. Sunderman, I. Barjoseph, N. Sauer, and T. Y. Chang, "Multiple quantum well passive mode locking of a NaCl color center laser," *Appl. Phys. Lett.*, vol. 54, pp. 1203–1205, 1989.

[3] U. Keller, W. H. Knox, and H. Roskos, "Coupled-cavity resonant passive mode-locked Ti-sapphire laser," *Opt. Lett.*, vol. 15, pp. 1377–1379, 1990.

[4] U. Keller, D. A. B. Miller, G. D. Boyd, T. H. Chiu, J. F. Ferguson, and M. T. Asom, "Solid-state low-loss intracavity saturable absober for Nd:YLF lasers—an antiresonant semiconductor Fabry–Perot saturable absorber," *Opt. Lett.*, vol. 17, pp. 505–507, 1992.

[5] U. Keller, K. J. Weingarten, F. X. Kärtner, D. Kopf, B. Braun, I. D. Jung, R. Fluck, C. Hönninger, N. Matuschek, and J. Aus der Au, "Semiconductor saturable absorber mirrors (SESAMs) for femtosecond to nanosecond pulse generation in solid-state lasers," *IEEE J. Sel. Topics Quantum Electron.*, vol. 2, no. 3, pp. 435–453, Sep. 1996.

[6] U. Keller, "Recent developments in compact ultrafast lasers," *Nature*, vol. 424, pp. 831–838, 2003.

[7] R. Szipőcs, K. Ferencz, C. Spielmann, and F. Krausz, "Chirped multilayer coatings for broadband dispersion control in femtosecond lasers," *Opt. Lett.*, vol. 19, pp. 201–203, 1994.

[8] F. X. Kärtner, N. Matuschek, T. Schibli, U. Keller, H. A. Haus, C. Heine, R. Morf, V. Scheuer, M. Tilsch, and T. Tschudi, "Design and fabrication of double-chirped mirrors," *Opt. Lett.*, vol. 22, pp. 831–833, 1997.

[9] F. Gires and P. Tournois, "Interféromètre utilisable pour la compression d'impulsions lumineuses modulées en fréquence," *C. R. Acad. Sci. Paris*, vol. 258, pp. 6112–6115, 1964.

[10] M. A. Duguay and J. W. Hansen, "Compression of pulses from a mode-locked He-Ne laser," *Appl. Phys. Lett.*, vol. 14, pp. 14–16, 1969.

[11] J. Heppner and J. Kuhl, "Intracavity chirp compensation in a colliding pulse mode-locked laser using thin-film interferometers," *Appl. Phys. Lett.*, vol. 47, pp. 453–455, 1985.

[12] J. Kuhl and J. Heppner, "Compression of femtosecond optical pulses with dielectric multilayer interferometers," *IEEE J. Quantum Electron.*, vol. QE–22, no. 1, pp. 182–185, Jan. 1986.

[13] D. Kopf, G. Zhang, R. Fluck, M. Moser, and U. Keller, "All-in-one dispersion-compensating saturable absorber mirror for compact femtosecond laser sources," *Opt. Lett.*, vol. 21, pp. 486–488, 1996.

[14] A. Isomäki, A.-M. Vainionpää, J. Lyytikäinen, and O. G. Okhotnikov, "Semiconductor mirror for optical noise suppression and dynamic dispersion compensation," *IEEE J. Quantum Electron.*, vol. 39, no. 11, pp. 1481–1485, Nov. 2003.

[15] M. Moenster, P. Glas, G. Steinmeyer, R. Iliew, N. Lebedev, R. Wedell, and M. Bretschneider, "Femtosecond neodymium-doped microstructure fiber laser," *Opt. Exp.*, vol. 13, pp. 8671–8677, 2005.

[16] M. Moenster, P. Glas, R. Iliew, R. Wedell, and G. Steinmeyer, "Microstructure soliton fiber laser," *IEEE Photon. Technol. Lett.*, vol. 18, no. 23, pp. 2502–2504, Dec. 2006.

[17] S. Hoogland, S. Dhanjal, J. S. Roberts, A. C. Tropper, R. Häring, R. Paschotta, F. Morier-Genoud, and U. Keller, "Passively modelocked diode-pumped surface-emitting semiconductor laser," *IEEE Photon. Techol. Lett.*, vol. 12, no. 9, pp. 1135–1137, Sep. 2000.

[18] A. Aschwanden, D. Lorenser, H. J. Unold, R. Paschotta, E. Gini, and U. Keller, "2.1-W picosecond passively mode-locked external-cavity semiconductor laser," *Opt. Lett.*, vol. 30, pp. 272–274, 2005.

[19] F. Saas, G. Steinmeyer, U. Griebner, M. Zorn, and M. Weyers, "Exciton resonance tuning for the generation of sub-picosecond pulses from a mode-locked semiconductor disk laser," *Appl. Phys. Lett.*, vol. 89, pp. 141107–1–141107–3, 2006.

[20] U. Keller and A. C. Tropper, "Passively modelocked surface-emitting semiconductor lasers," *Phys. Rep.*, vol. 429, pp. 67–120, 2006.

[21] M. Whitehead, A. Rivers, G. Parry, J. S. Roberts, and C. Button, "Low-voltage multiple quantum well reflection modulator with on:off ratio $>$100:1," *Electron. Lett.*, vol. 25, pp. 984–985, 1989.

[22] E. Garmire, "Analytic performance analysis based on material properties for electroabsoprtive asymmetric Fabry–Perot reflection modulators," *Appl. Opt.*, vol. 41, pp. 1574–1583, 2002.

[23] A. Yariv, "Critical coupling and its control in optical waveguide-ring resonator systems," *IEEE Photon. Technol. Lett.*, vol. 14, no. 4, pp. 483–485, Apr. 2002.

[24] G. Steinmeyer, "Dispersion oscillations in ultrafast phase correction devices," *IEEE J. Quantum Electron.*, vol. 39, no. 8, pp. 1027–1034, Aug. 2003.

[25] G. Stibenz, G. Steinmeyer, and W. Richter, "Dynamic spectral interferometry for measuring the nonlinear amplitude and phase response of a saturable absorber mirror," *Appl. Phys. Lett.*, vol. 86, pp. 081105-1–081105-3, 2005.

[26] M. Haiml, R. Grange, and U. Keller, "Optical characterization of semiconductor saturable absorbers," *Appl. Phys. B*, vol. 79, pp. 331–337, 2004.

[27] A. Gosteva, M. Haiml, R. Paschotta, and U. Keller, "Noise-related resolution limit of dispersion measurements with white-light interferometers," *J. Opt. Soc. Amer. B*, vol. 22, pp. 1868–1874, 2005.

[28] F. Reynaud, F. Salin, and A. Berthelemy, "Measurement of phase shifts introduced by nonlinear optical phenomena on subpicosecond pulses," *Opt. Lett.*, vol. 14, pp. 275–277, 1989.

[29] L. Lepetit, G. Chériaux, and M. Joffre, "Linear techniques of phase measurement by femtosecond spectral interferometry for applications in spectroscopy," *J. Opt. Soc. Amer. B*, vol. 12, pp. 2467–2474, 1995.

[30] Scientific Computing International, Software Program "Film Wizard". Carlsbad, CA [Online]. Available: http://www.sci-soft.com

[31] A. Thelen, *Design of Optical Interference Coatings*. New York: McGraw-Hill, 1989.

[32] B. C. Collings, K. Bergman, S. T. Cundiff, S. Tsuda, J. N. Kutz, J. E. Cunningham, W. Y. Jan, M. Koch, and W. H. Knox, "Short cavity erbium/ytterbium fiber lasers mode-locked with a saturable bragg reflector," *IEEE J. Sel. Topics Quantum Electron.*, vol. 3, no. 4, pp. 1065–1075, Aug. 1997.

[33] D. H. Sutter, G. Steinmeyer, L. Gallmann, N. Matuschek, F. Morier-Genoud, U. Keller, V. Scheuer, G. Angelow, and T. Tschudi, "Semiconductor saturable-absorber mirror-assisted Kerr-lens mode-locked Ti:sapphire laser producing pulses in the two-cycle regime," *Opt. Lett.*, vol. 24, pp. 631–633, 1999.

[34] F. X. Kärtner and U. Keller, "Stabilization of solitonlike pulses with a slow saturable absorber," *Opt. Lett.*, vol. 20, pp. 16–18, 1995.

Mathias Moenster received the diploma degree in electrical engineering from RWTH Aachen University, Aachen, Germany, in 2002. He is currently working towards the Ph.D. degree at the Max-Born-Institute, Berlin, Germany.

He was with the Heinrich-Hertz-Institute, Berlin, Germany, before joining the Max-Born-Institute in 2003. His current research interest is focused on femtosecond fiber lasers and microstructure fibers.

Uwe Griebner received the Ph.D. degree in physics from the Technical University of Berlin, Berlin, Germany, in 1996. His Ph.D. research was on fiber bundle lasers with high average power.

Since 1992, he has been with the Max-Born-Institute, Berlin, Germany, working on diode pumped solid-state lasers, fiber lasers, waveguide lasers, microoptics, microoptics for special resonators, and ultrafast lasers. He is currently focused on ultrafast diode-pumped solid-state lasers and amplifiers applying new active materials and the use of micro-optical components for femtosecond beam-shaping.

Wolfgang Richter was born in Zeitz, Germany, in 1942. He received the Diploma in physics from Technical University, Dresden, Germany, in 1968, and the PhD. and the Habilitation degree from the University of Jena, Jena, Germany, in 1972 and 1981, respectively.

In 1969, he began research in the field of superconductivity at the University of Jena, Jena, Germany. In 1992, he became Professor of experimental physics at the University of Jena and is working in the field of semiconductor physics and optoelectronics. In 2003, he founded BATOP GmbH, Weimar, Germany, which produces nonlinear semiconductor optical devices.

Günter Steinmeyer (M'96) was born in Bad Pyrmont, Germany, in 1965. He received the Diploma the Ph.D. degree from Hannover University, Hannover, Germany, in 1991 and 1995, respectively, and the Habilitation degree from Swiss Federal Institute of Technology (ETH), Zürich, in 2002.

In 1995, he joined the Research Laboratory of Electronics at the Massachussets Institute of Technology, Cambridge, where he worked on ultrafast spectroscopy and photonic bandgap structures. In 1998 he moved to ETH to work on few-cycle pulse generation, pulse characterization, and chirped mirror design. In July 2002, he moved to the Max-Born-Institute, Berlin, Germany.

Dr. Steinmeyer is a member of the Optical Society of America and the German Physical Society.